Title	Modeling of Zircaloy cladding primary creep during load drop and reversal
Author(s)	Tulkki, Ville; Ikonen, Timo
Citation	Journal of Nuclear Materials. Vol. 445 (2014) No: 1 - 3, Pages 98 - 103
Date	2014
URL	http://dx.doi.org/10.1016/j.jnucmat.2013.10.053
Rights	This is a pre-print version of the published article. This article may be downloaded for personal use only.

Modelling of Zircaloy cladding primary creep during load drop and reversal

V. Tulkki*, T. Ikonen

VTT Technical Research Centre of Finland, P.O.Box 1000, 02044 VTT Finland

Abstract

Modelling fuel behaviour requires an accurate description of the cladding stress response for both operational and safety considerations. The transient creep response of Zirconium alloys is commonly modelled using a strain hardening rule which is known to hold in cases with monotonously increasing stresses. However, the strain hardening rule is experimentally known to fail in scenarios such as load drop or reversal.

In this paper we derive a simple and easily implementable set of rules for primary creep based on experimental results which contradict the strain hardening rule. The primary creep predicted by these rules is compared with data from published thermal creep experiments and Halden in-pile creep experiment IFA-585. The model thus created is shown to perform well in describing both transient stress scenarios with monotonously increasing stress and scenarios involving load drops and reversals.

Keywords: Zircaloy, creep modelling, transient response, hardening law

1. Introduction

The cladding of a fuel rod contains the radioactive fission products produced during the time the rod is in the reactor. During its reactor life the cladding tube is under a pressure differential at elevated temperatures and under irradiation. These conditions cause the cladding to creep, first inwards as the reactor system pressure exceeds the fuel internal pressure, and then outwards as the expanding pellet pushes the cladding. The reactor operation

*Tel. +358 20 722 6114; fax +358 20 722 7001.
E-mail address: ville.tulkki@vtt.fi

causes additional alternating stresses, to which the cladding must conform. At high burnup the rod internal overpressure may even push the cladding to creep faster than the fuel pellet swells, potentially creating a self-reinforcing cladding lift-off effect [1] which may lead to fuel failure. It is therefore important to be able to describe the creep behaviour of the cladding adequately.

Conventionally creep is described by having three regions: the primary (or transient) region, the secondary steady state region and the third leading to failure. As the fuel rods stay in the reactor only for limited time, most of the models used describe the first two regions. The extension to the rupture becomes important in studies such as spent fuel behaviour in interim dry storage conditions, which is outside the scope of this work. The correlations are matched to experiments with a single stress increase, and the change of stress encountered in fuel behaviour analysis is handled by hardening laws. Typically the creep in metals follows either a time or a strain hardening law, and the latter is usually assumed to hold for Zirconium alloys in usual operating conditions [2].

Various creep correlations have been formulated over the years that take both thermal and irradiation creep into account. It is well known that the hardening laws used to take the transient conditions into account are simplifications and do not apply universally. Stress reversal and stress reduction are special situations where the hardening laws fail. These situations have been successfully described with complex formulations of cladding material thermodynamic states [3, 4] and by assuming additional deformation terms such as reversible anelastic deformation [5, 6]. While these formulations appear to provide correct prediction of the cladding creep behaviour they are not commonly implemented in fuel behaviour codes due to their complexity. Fuel behaviour analysis is commonly performed with integral codes utilizing separate models to describe various phenomena, and the number of required simulations may rise to hundreds of thousands of fuel rod simulations depending on the application [7, 8]. For this purpose, a simple and more practical approach is needed.

In this paper we present a simple primary creep formulation to describe cladding creep response to transient stresses based on previously published experimental data [9, 10]. The resulting model is both able to handle the situations where strain hardening law fails as well as to closely replicate strain hardening in situations where it has been experimentally shown to hold.

The structure of the paper is as follows. In Section 2, we discuss the experimental basis for the current creep modelling and derive the new model

based on the experimental results. The model is verified against experimental data in Section 3 and the results of the paper are summarized in Section 4.

2. Theory

2.1. Background

While the creep of Zircaloy alloys has been studied extensively (e.g. Refs. [11, 12, 13, 14, 15, 16, 17, 18, 19, 20]), only a few published experiments have concentrated on the response to complex transients. According to investigations of Lucas and Pelloux [2] the thermal creep deformation at temperatures below 375 °C can be described by a strain hardening rule. In strain hardening it is assumed that the creep response always follows a curve as seen in single stress level experiments and the changing stress state is taken into account by moving to the new stress/strain curve to the point where accumulated strain is retained. This work is used as a justification for the use of the strain hardening rule in most of the models [10, 15, 21]. Matsuo investigated thermal creep of Zircaloy-4 [12] and formulated a correlation, which Limbäck and Andersson extended to reactor conditions [21].

Murty and Yoon investigated strain transients following stress changes [5] and proposed a creep model which assumes an anelastic strain component in addition to the traditional elastic and plastic contributions. This aneslastic component is used to succesfully explain the observed accumulation of reverse strain at load drop, while the traditional plastic contribution from creep is assumed to follow the strain hardening rule. Matsuo also investigated the creep behaviour of Zircaloy under variable conditions [10] and formulated a set of rules for stress reversal situations based on reversible creep hardening surfaces.

A common assumption in the creep models utilized in the integral fuel behaviour codes is that the creep strain ϵ can be divided into two parts, primary ϵ_p and secondary ϵ_s:

$$\epsilon = \epsilon_p + \epsilon_s. \tag{1}$$

The secondary steady state part usually consists of thermal and irradiation creep contributions ($\dot{\epsilon}_s = \dot{\epsilon}_{th} + \dot{\epsilon}_{irr}$), such as in the fuel performance code FRAPCON-3.4's correlation [22, 23, 24] which is effectively the model by Limbäck and Andersson [21] modified to use effective stress σ_{eff} instead of hoop stress:

$$\dot{\epsilon}_{th} = A\frac{E}{T}(\sinh\frac{a_i\sigma_{\text{eff}}}{E})^n e^{-\frac{Q}{RT}} \text{ and} \tag{2}$$

$$\dot{\epsilon}_{irr} = C_0 \cdot \phi^{C_1} \cdot \sigma_{\text{eff}}^{C_2} \cdot f(T), \tag{3}$$

where E is the elastic modulus, T is temperature in K, R is the universal gas constant, Q the activation energy of the creep, ϕ the fast neutron flux ($\text{n/m}^2\text{s}^{-1}$). The variables A, a_i, n, C_i and the function $f(T)$ have different values depending on the cladding type and the environment as described in Ref. [24]. The use of σ_{eff}

$$\sigma_{\text{eff}} = \sqrt{0.5((\sigma_a - \sigma_h)^2 + (\sigma_h - \sigma_r)^2 + (\sigma_r - \sigma_a)^2)} \tag{4}$$

is justified by an improved modelling of tensile and compressive creeps [24]. Here $\sigma_{a,h,r}$ denote stresses in axial, hoop and radial directions and isotropic behaviour is assumed for simplicity.

Limbäck and Andersson assume that the form of the primary creep is similar to the one proposed by Matsuo [12], in particular of the form

$$\epsilon_p = \epsilon_p^S (1 - e^{f(\dot{\epsilon}_s t)}), \text{and} \tag{5}$$

$$\epsilon_p^S = B \cdot \dot{\epsilon}_s^b, \tag{6}$$

where the saturated primary creep ϵ_p^S is related to secondary creep rate with constants B and b, and the time for primary creep to saturate is a function $f(\dot{\epsilon}_s t)$ of the secondary creep rate. The transient stress is taken into account by assuming a strain hardening rule.

However, these models are contradicted by the results of the Halden in-pile creep experiment IFA-585 [9]. According to the experiment it would appear that the primary creep depends on the direction of stress change while the secondary creep rate depends on the stress level. This is in contrast to the model of Eq. (6) which assumes that the magnitude of saturated primary creep is proportional to the secondary creep rate.

2.2. Formulation of new creep correlation

In this work we focus on the response to transient stresses. The model for the primary creep $\epsilon_p(t)$ is derived on a phenomenological basis, most importantly requiring consistency with the experimental results reported for IFA-585 [9, 25]. According to the experiment, the total saturated primary creep is proportional to the change in the applied stress. The primary creep strain due to one stress change can then be approximately described by a function of the form

$$\epsilon_p(t) = C(\sigma_1 - \sigma_0)(1 - e^{-\frac{t-t_0}{\tau}}) \tag{7}$$

where C is a constant, σ_0 and σ_1 are the initial and final externally applied stresses, respectively, t_0 is the time when the change of stress from its initial to final value occurs, and τ is the characteristic time scale of the primary creep.

To utilize the experimental results (Eq. (7)) in a practical scenario with several sequential stress changes, one needs a way to keep record of the stress history of the system. In response to the changing stress, the material evolves through a complex set of internal states, with $\epsilon_p(t)$ slowly approaching the saturation value. We propose that to reproduce the behavior of Eq. (7), it is sufficient to characterize the internal state of the system by a single time-dependent stress-like variable, $\sigma_{int}(t)$. The time evolution of σ_{int} describes the relaxation of the internal state of the system towards the steady state determined by the externally applied stress. We choose the scale of σ_{int} so that for an initial state with zero primary creep rate and the applied stress is equal to σ_0, $\sigma_{int}(t = t_0) = \sigma_0$. As the applied stress is changed to σ_1, the variable σ_{int} starts to evolve in time, approaching the new steady state value $\sigma_{int}(t \to \infty) = \sigma_1$, which is reached when the primary creep has fully saturated.

In order to find the time evolution of $\sigma_{int}(t)$ at intermediate times, we make an *ansatz* of a simple linear response, so that the strain rate is given by

$$\frac{d\epsilon_p(t)}{dt} = D(\sigma_1 - \sigma_{int}(t)). \tag{8}$$

Thus, the relaxation of σ_{int} towards the saturation value σ_1 ultimately determines the rate of primary creep. In the conventional approach, one would determine $\sigma_{int}(t)$ using thermodynamics or microscopic arguments, and use a relation such as Eq. (8) to derive the primary creep strain as a function of time. However, in deriving the phenomenological model, we take the reverse approach. We require that the experimental result of Eq. (7) holds for $\epsilon_p(t)$ and use Eq. (8) to derive $\sigma_{int}(t)$. The result is

$$\sigma_{int}(t) = \sigma_1 - (\sigma_1 - \sigma_0)e^{-\frac{t-t_0}{\tau}}, \tag{9}$$

also fixing the constant $D = C/\tau$ in Eq. (8).

Equations (7) and (9) can be cast in a form that has no explicit dependence on the initial values σ_0 and t_0. If the strain and internal stress have

known values $\epsilon_p(t)$ and $\sigma_{int}(t)$ at time t, the corresponding values at time $t + \Delta t$ are given by

$$\epsilon_p(t + \Delta t) = \epsilon_p(t) + C(\sigma_{ext} - \sigma_{int}(t))(1 - e^{-\frac{\Delta t}{\tau}}), \tag{10}$$

$$\sigma_{int}(t + \Delta t) = (\sigma_{int}(t) - \sigma_{ext})e^{-\frac{\Delta t}{\tau}} + \sigma_{ext}, \tag{11}$$

where the notation σ_{ext} has been used for the externally applied stress (σ_1). Equations (10) and (11), together with the initial conditions $\sigma_{int}(t_0) = \sigma_0$ and $\epsilon_p(t_0) = 0$, constitute the phenomenological creep model.

By keeping record of the time evolution of the system's internal state via σ_{int}, the model can take into account fast consecutive stress changes, even when the primary creep does not saturate between them. It is also easy to verify that Eq. (7) is recovered in the limit of a single stress change from σ_0 to σ_1. From the practical point of view, it is important that written in the form of Eqs. (10) and (11), the model only requires knowledge of σ_{int} at the previous time step to calculate the incremental ϵ_p, making its implementation into a fuel performance code straightforward. Also note that Eqs. (10) and (11) are exact, although they have the appearance of a finite difference approximation.

The variables C and τ of Equations (10) and (11) depend on both manufacturing properties of the cladding materials and the environment (temperature, neutron flux, etc.). A complete creep correlation would require determination of these dependencies with well characterized materials [12, 21]. However, this is out of the scope of this paper, where our aim is to demonstrate the applicability of the new hardening rule in principle. As it is, we consider both C and τ as parameters to be determined from experimental data.

2.3. Mechanical analogue

In addition to creep, a system has an elastic response to external stress. Including the elastic strain ϵ_{el} in Eq. (1), the total strain due to external stress can be written as

$$\epsilon = \epsilon_{el} + \epsilon_p + \epsilon_s. \tag{12}$$

In Eq. (12), the primary creep ϵ_p has a saturation value, while the secondary creep is assumed to grow without limit under applied stress. Such a system can be approximately described by a mechanical analogue displayed in Figure 1. The springs A and B are elastic components whose displacement

$\epsilon_{\text{spring}} = \sigma/\kappa_i$, where κ_i is the elastic modulus of spring i and σ is the external stress affecting the given component, while the dashpots C, D and E represent viscous elements with a rate of displacement of $\dot{\epsilon}_{\text{dashpot}} = \sigma/\eta_i$, where η_i is the viscosity of the dashpot i. The nodes A, B and C create a model known as standard linear solid (SLS) model which is commonly used in viscoelastic studies due to its ability to describing both creep and relaxation behaviour of many materials [26]. The SLS part in this analogue models the elastic response and the primary creep, and the twin dashpots D and E the thermal and irradiation steady state creep.

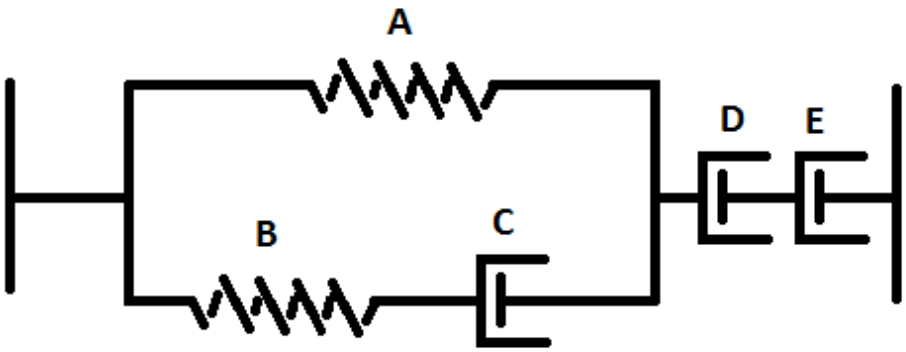

Figure 1: Mechanical analogue for the proposed creep model.

The solution to SLS is well known [26], and the solution of the whole system with the the dashpots D and E in a series is obtained by simple addition. The solution to the strain as a function of applied stress $\sigma(t)$ is of the form

$$\begin{aligned}\epsilon(t) - \epsilon(0) =& \frac{\sigma(t) - \sigma(0)}{\kappa} + \\ & \int_0^t C\left(1 - e^{-\xi/\tau}\right)\frac{d\sigma(\xi)}{d\xi}d\xi + \\ & \left(\frac{1}{\eta_D} + \frac{1}{\eta_E}\right)\int_0^t \sigma(\xi)d\xi, \end{aligned} \tag{13}$$

with the constants κ, C and τ being functions of κ_i and η_C. The first term corresponds to the elastic strain, the second to primary creep, and the last one to secondary creep (both thermal and irradiation induced).

In the case of an instantaneous stress change from σ_0 to σ_1 at time $t = t_0$, the derivative $d\sigma(t)/dt = (\sigma_1 - \sigma_0)\,\delta(t - t_0)$, with δ the Dirac delta distribution, Eq. (13) reduces to Eq. (7) for the primary creep. For several stepwise changes, Eqs. (10) and (11) can be recovered. In addition, the response to a more general change in stress can be solved from Eq. (13). Thus, while the primary creep model was derived from an experimental basis, it also has a direct mechanical analogue that is easy to interpret and whose mathematical properties are well known.

3. Experimental verification

The primary creep formulation was tested against published sets of variable stress data. First, we show the model behaviour against the Zircaloy-2 BWR rod of IFA-585 Halden experiment [9] whose results were the basis of the model formulation. The amount of published in-pile creep experiments with on-line monitoring is scarce, and therefore the second set was chosen to be the experiments on Zircaloy-4 samples by Matsuo [12]. Due to the different experimental setups (different materials, in-pile and out-of-pile experiment) different creep correlations were used for the two sets. For analysis of the Matsuo's out-of-pile tests the secondary creep part was modelled after the correlation by Matsuo [12]:

$$\epsilon_s = 1.57 \times 10^{13} \frac{E}{T} (\sinh \frac{1.13 \times 10^3 \sigma_h}{E})^{2.1} e^{-\frac{2.72 \times 10^5}{RT}} \tag{14}$$

where elastic modulus $E = 1.148 \times 10^5 - 59.9T$ MPa. For the in-pile IFA-585 the secondary creep was modelled as per FRAPCON-3.4's modified Limbäck and Andersson model of Eqs. (2) and (3) with the variables set as described in Ref. [24] for RXA cladding. Eqs. (10) and (11) were used for primary creep with values of σ_{int}, C and τ described in the following subsections.

3.1. Halden in-pile experiment IFA-585

The OECD/NEA IFPE data for IFA-585 experiment [27] was used for the in-pile experiment. In the IFA-585 experiment a pre-irradiated BWR cladding tube was pressurized to several stress states, both compressive and tensile, while under irradiation in the Halden research reactor. The cladding deformation was measured with on-line diameter gauges which were calibrated to unpressurized reference diameters on the end plugs. There was also a composite PWR rod in the test but as the diameter measurements

were reported [28] to be anomalous relatively early on in the experiment we focus on the BWR sample in this paper.

The BWR rod sample was irradiated prior to the Halden experiment in a commercial reactor to a fast neutron dose of 6×10^{21} n/cm^2. Also, during the first experimental cycle there were issues with rod pressurization which are not included in the analysis. For the simulations shown here it has been assumed that $\sigma_{int} = -52$ MPa at $t = 0$, which was the planned effective stress on the cladding in the initial cycle. The value of $C = 1.92 \times 10^{-6}$ m^2/N is as per Ref. [9] and $\tau = 100$ h was chosen by fitting to the data.

There are uncertainties in the test results [29], especially related to the effect of the different rates of oxide layer growth between the sample and the end plugs and experimentally derived secondary creep rate [25]. In the following the simulated secondary creep rate is altered by the same amount as the experimental measurement is reported to be affected by the differential in the oxide layer growth rates [25]. For secondary creep it has been noted that IFA-585 experiment features very high secondary creep rates [25] compared to other creep experiments such as those of Ref. [15]. This was also seen in the initial analysis. The FRAPCON correlation used for secondary creep rate was multiplied by a factor of 2 in order to better match the experimental results. Neither of these two uncertainties should change the interpretation of the behaviour of the primary creep.

The comparison between the simulated and measured inelastic deformation, along with the applied effective stress for IFA-585 experiment, is shown in Fig. 2. The mid-wall effective stress with positive values signifying tension and negative values compression is also shown in Fig. 2. The match between the experiment and the simulation is good, especially at the beginning of the experiment. However, errors mostly due to the uncertainties in the secondary creep rate compound during the simulation. In Fig. 3 only the initial inelastic deformation after each stress step is shown and the plotting of the deformation at the beginning of each stress step is shifted to zero. The results show excellent agreement between the simulated and measured behaviour. Thus it can be argued that the error seen in Fig. 2 is mostly due to the uncertainty in the secondary creep rate, and that the creep response to stress reversal can be modelled using the Eqs. (10) and (11).

3.2. Matsuo's out-of-pile experiments

For examining the Matsuo's out-of-pile tests the experimental data points were extracted from Figures 3, 4, 7 and 9 of Ref. [10]. The data details creep

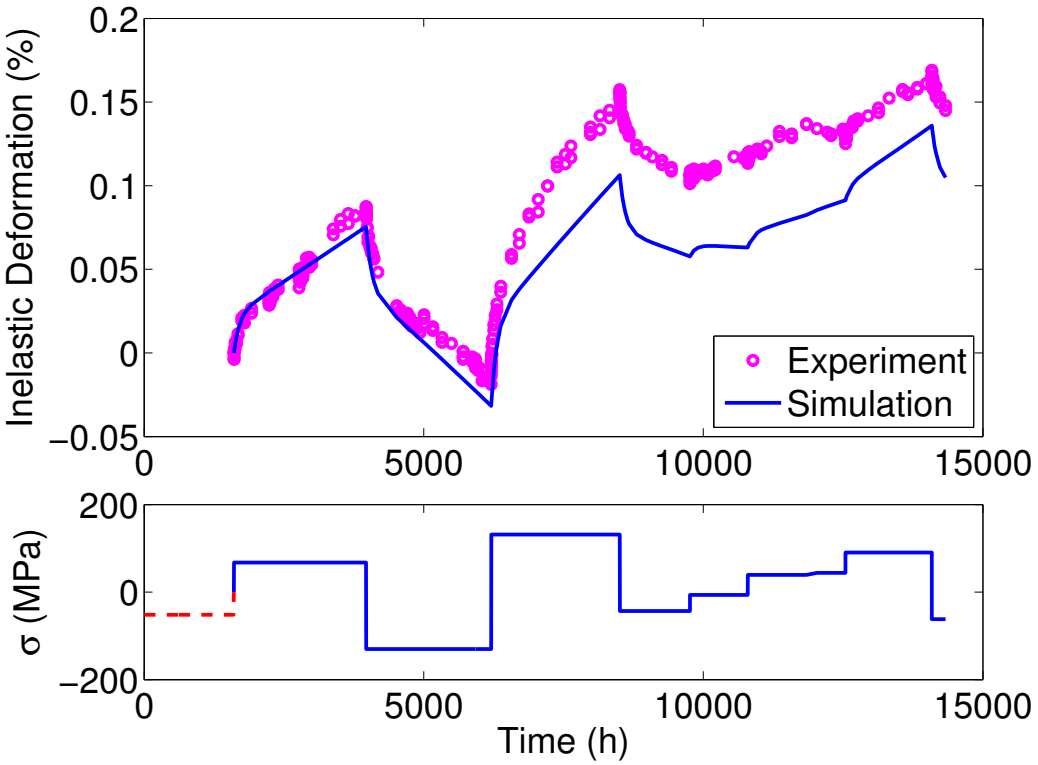

Figure 2: IFA-585 BWR experiment (circles) and simulated behaviour (line). The applied stress history is displayed in the bottom plot.

behaviour during load increase from 77.9 MPa to 148.1 MPa of tensile hoop stress, load drop from 156.9 MPa to 74.3 MPa of tensile hoop stress and two series of load reversal steps alternating between tensile hoop stress of 148 MPa and compressive hoop stress of 78 MPa. Cladding temperature during these tests was 662.9–664.0 K. Matsuo uses cladding tube hoop stress in his analysis and correlations, and thus hoop stress instead of effective stress is used when analysing these experiments. The tests are pressurized tube tests with biaxial stress condition $\sigma_a/\sigma_h = 1/2$ [10] yielding $\sigma_{\text{eff}} = \sqrt{3}/2\sigma_h$ according to Eq. (4). The difference between using hoop and effective stress in analysing the primary creep behaviour in this experimental arrangement is seen only in the value of the parameter C.

For Matsuo's experiments the fitting parameters were set as $C = 3.8 \times 10^{-5}$ m^2/N and $\tau = 40$ h. For the simulations shown here it has been assumed that $\sigma_{int} = 0$ at $t = 0$. Also, an improved match to the results was gained by

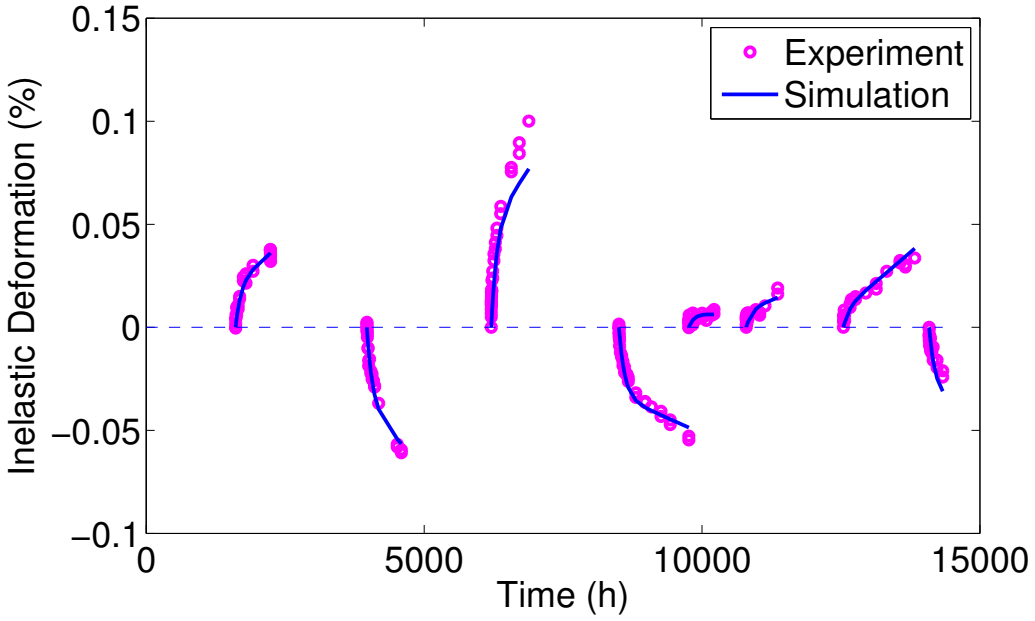

Figure 3: The model behaviour against measurements for the beginning of each stress step. The plots start at $\epsilon = 0$ at the beginning of each pressure step.

multiplying Eq. (14) by a factor of 1.25. The results are shown in Figures 4–7 as the *baseline* line. While for Fig. 4 the match is good, the experiments with load reversals, depicted in Figures 6 and 7, demonstrate the need for additional assumptions. The primary creep during the subsequent stress steps was clearly smaller than during the initial primary creep stage. Matsuo uses in his work a concept of creep hardening surface [10]. In our model, similar improvement can be achieved by assuming that there are hardening processes which decrease the saturated primary creep by half during primary creep re-initiation. With such an assumption, simulation results according to the *hardening* line in Figs. 4–7 were achieved.

Figure 4 shows the results of a test where the hoop stress was first set at $\sigma_h = 77.9$ MPa and then increased to $\sigma_h = 148.1$ MPa. The match between the experiment and simulation is good, and here the effect of the hardening is not overly clear. It should be noted that this kind of experiment, where the stress is increased, is where the strain hardening rule provides good results. As seen here, the model proposed in this paper provides similar behaviour to strain hardening rule in cases where stress is increased in subsequent steps.

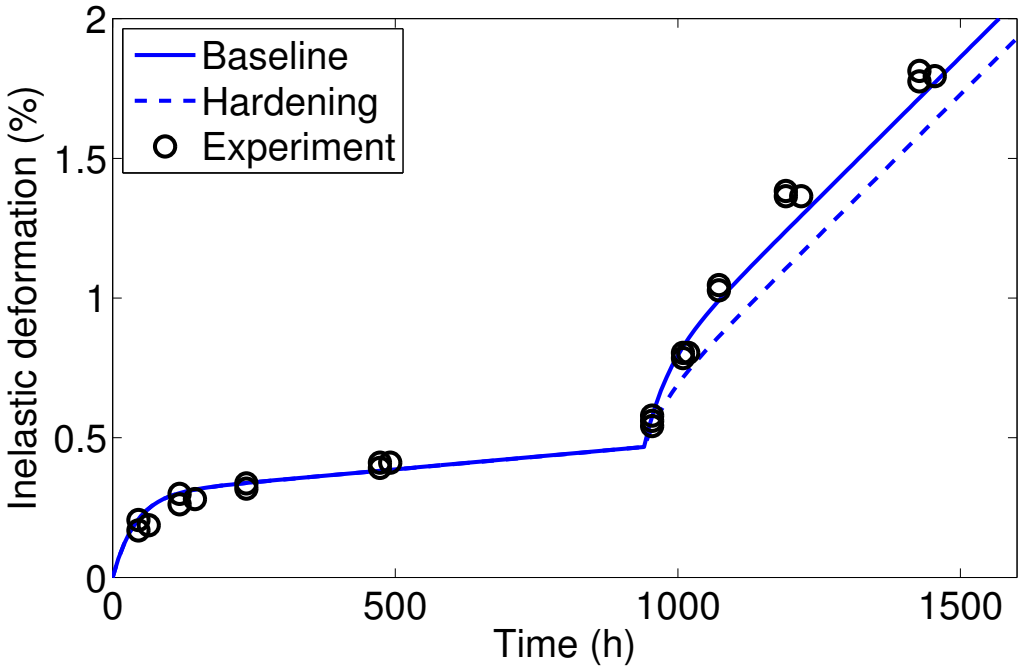

Figure 4: Simulated (lines) and experimental (circles) cladding response to stress increase. Experimental data from Figure 3 of Ref. [10].

Figure 5 shows the results of a test where the hoop stress was first set $\sigma_h = 156.9$ MPa and then decreased to $\sigma_h = 74.3$ MPa. Matsuo noted that a certain amount of strain recovery was observed just after the load drop [10], which is also shown by the new model. The strain recovery phenomenon is documented also by Murty [5]. The discrepancy between the simulation and the experiment can be mostly attributed to a slightly too low secondary creep rate.

Figures 6 and 7 show results of two experiments where the load was alternated between tension ($\sigma_h = 148.1$ MPa) and compression ($\sigma_h = -78.0$ MPa). Here the need for assuming some hardening behaviour in primary creep is evident. The other alternative would be to assume initial σ_{int} to be of the order of -150 MPa due to manufacturing or test setup effects which would increase the initial primary creep relative to subsequent stress steps. However, such a large value for the initial σ_{int} is considered improbable. The match between the experiment and simulation is good, therefore demonstrating the applicability of the proposed model in load reversal situations. The need for a

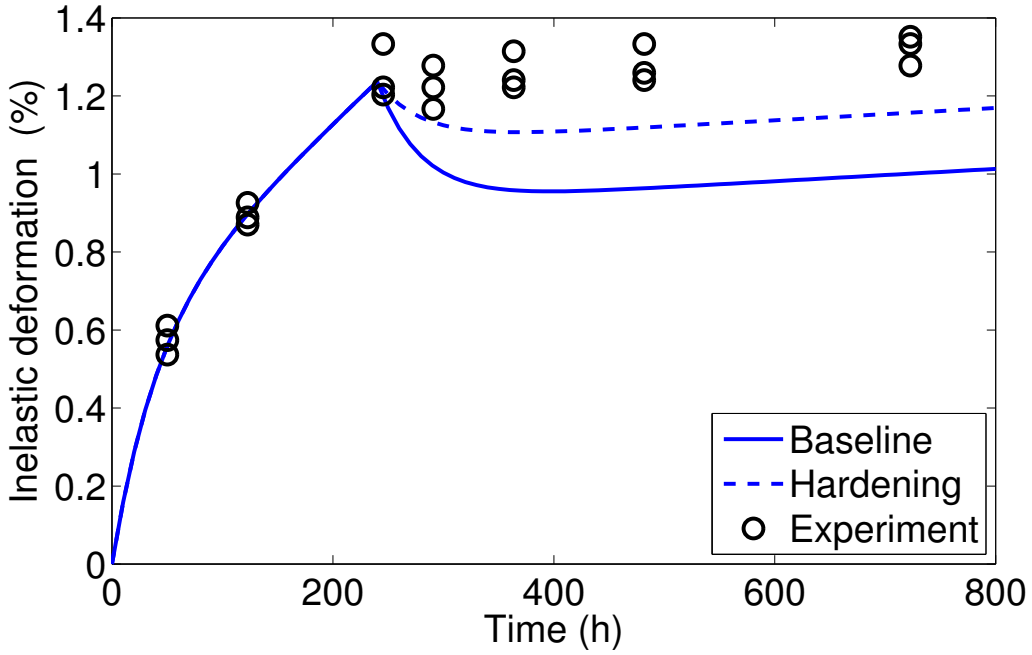

Figure 5: Simulated (lines) and experimental (circles) cladding response to load drop. Experimental data from Figure 4 of Ref. [10].

hardening assumptio,n which was not needed in the IFA-585 analysis, raises a question whether the Zircaloy primary creep behaviour during in-pile and out-of-pile experiments are equivalent.

4. Conclusions

In this paper simple and easily implementable rules, Eqs. (10) and (11), for the primary creep behaviour of Zircaloy cladding were derived based on in-pile results from Halden IFA-585 creep experiment. A creep model using these rules is capable of replicating observed behaviour during stress reversal and load drop situations required in fuel behaviour codes. In scenarios where a commonly used strain hardening rule is known to work, such as stress increases, the current model behaves similarly to other strain hardening models. However, instead of hardening to strain, the new model effectively relaxes to current externally imposed stress state.

Most of the stresses imposed to the cladding in IFA-585 were low enough for the creep rate to depend linearly on the stress. Therefore the model is

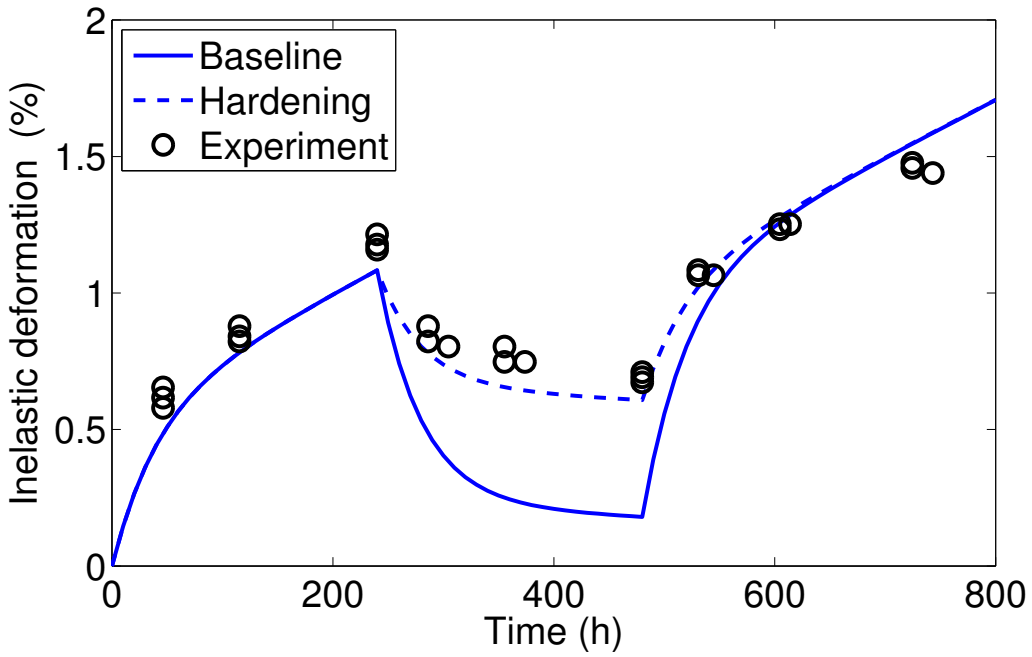

Figure 6: Simulated (lines) and experimental (circles) cladding response to stress reversal. Experimental data from Figure 7 of Ref. [10].

most applicable to low stress situations such as the normal reactor operation. The applicability to thermal creep experiments was also demonstrated. Different model parameters were required for the tests. For the parameter C describing the stress/strain-relation, the ratio of used values is approximately 20. This can be argued to be due to differences in test temperatures, which were 575–595 K for IFA-585 and 662.9–664.0 K for Matsuo's experiments. The characteristic times, τ, for the primary creeps differed also, 40 h for Matsuo experiments and 100 h for IFA-585. The faster kinetics could be attributed to higher temperature. Different materials and experimental conditions do affect the results also. These relationships should be investigated further in order to create a full creep model implementable to a fuel behaviour code.

The comparisons between the thermal creep experiments show a difference in the primary creep re-initiation behaviour between in-pile and out-of-pile experiments. This is significant as most variable stress experiments are performed out-of-pile whereas the application, the modelling of nuclear

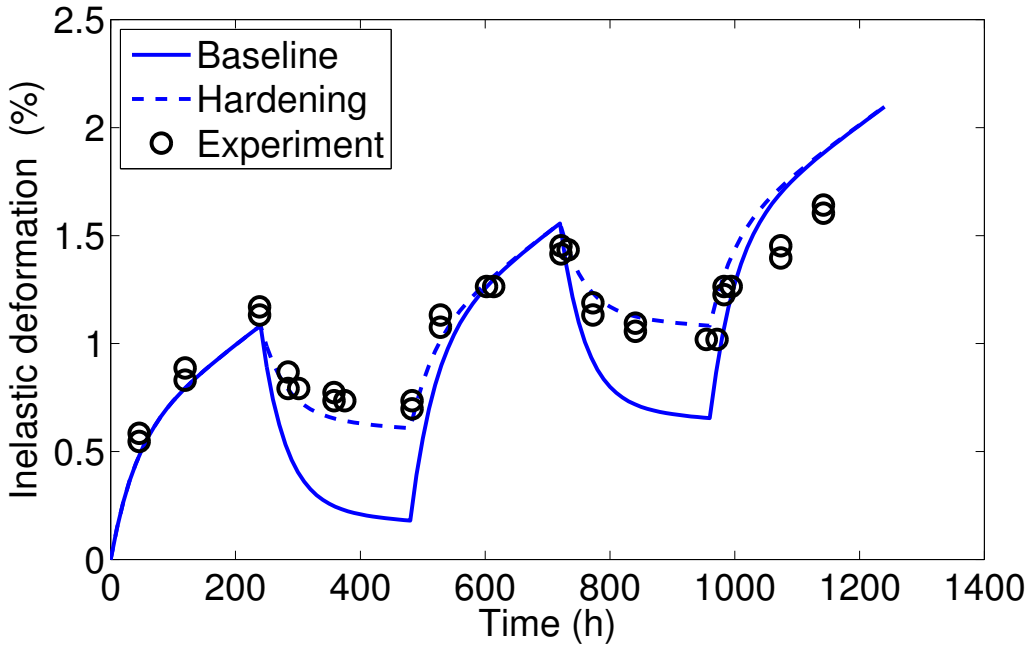

Figure 7: Simulated (lines) and experimental (circles) cladding response to stress reversal. Experimental data from Figure 9 of Ref. [10].

fuel in reactor, requires a correct description of the in-pile behaviour. Unfortunately, there are few published in-pile creep experiments with transient stress states.

The cladding of the nuclear fuel experiences varying conditions during its reactor life, from compressive stresses during initial reactor cycles to tensile stress imposed by the expanding fuel pellets and increasing rod internal pressure. Accurate modelling of the cladding stress response to transient stresses is important for both operational and safety considerations. The rules derived in this paper provide new insight into how the stress transients can be treated.

Acknowledgements

This work was partially funded by SAFIR2014, the Finnish Research Programme on Nuclear Power Plant Safety 2011-2014, and Academy of Finland funded IDEA project. The model development was carried out in cooperation with Halden Reactor Project.

References

[1] W. Wiesenack, T. Tverberg, M. McGrath, E. Kolstad, S. Beguin, Journal of Nuclear Science and Technology 43 (2006) 1037–1044.

[2] G. Lucas, R. Pelloux, Nuclear Technology 53 (1981) 46–57.

[3] D. Lee, F. Zaverl, E. Plaza-Meyer, Journal of Nuclear Materials 88 (1980) 104–110.

[4] L. Jernkvist, Transactions of the 15th International Conference on Structural Mechanics in Reactor Technology (SMiRT-15) C04/3 (1999) 477–484.

[5] K. Murty, K. Yoon, Transactions of the 5th International Conference on Structural Mechanics in Reactor Technology (SMiRT-5) C3/6 (1979).

[6] K. Murty, JOM 51 (1999) 32–39.

[7] T. Ikonen, V. Tulkki, Submitted to Nuclear Engineering and Design (2013).

[8] G. Rossiter, Nuclear Engineering and Technology 43 (2011) 489–498.

[9] M. McGrath, HWR-471 (1996).

[10] Y. Matsuo, ASTM STP 1023 (1989) 678–691.

[11] D. Franklin, G. Lucas, A. Bement, ASTM STP 815 (1983).

[12] Y. Matsuo, Journal of Nuclear Science and Technology 24 (1987) 111–119.

[13] F. Garzarolli, H. Stehle, E. Steinberg, ASTM STP 1295 (1996) 12–32.

[14] Y. S. Kim, Journal of Nuclear Materials 250 (1997) 164–170.

[15] A. Soniak, N. L'Hullier, J.-P. Mardon, V. Rebeyrolle, P. Bouffioux, C. Bernaudat, ASTM STP 1423 (2002) 837–862.

[16] K. Ito, K. Kamimura, Y. Tsukuda, Proceedings of the 2004 International Meeting on LWR Fuel Performance (2004) 440–451.

[17] M. Griffiths, N. Christodoulou, S. Donohue, ASTM STP 1467 (2005) 686.

[18] J. Moon, P. Cantonwine, K. Anderson, S. Karthikeyan, M. Mills, Journal of Nuclear Materials 353 (2006) 177–189.

[19] R. Holt, Journal of Nuclear Materials 372 (2008) 182–214.

[20] H. Wang, Z. Hu, W. Lu, M. Thouless, Journal of Nuclear Materials 433 (2013) 188–198.

[21] M. Limback, T. Andersson, ASTM STP 1295 (1996) 448–468.

[22] K. Geelhood, Nuclear Engineering and Technology 43 (2011) 509–522.

[23] K. Geelhood, W. Luscher, C. Beyer, NUREG/CR-7022, Vol.1 (2011).

[24] W. Luscher, K. Geelhood, NUREG/CR-7024 (2011).

[25] J. Foster, M. McGrath, Proceedings of the 2007 LWR Fuel Performance Meeting (2007).

[26] H. Banks, S. Hu, Z. Kenz, Advances in Applied Mathematics and Mechanics 3 (2011) 1–51.

[27] IFPE database NEA IFPE/IFA-585 experimental data, . Last modified 13-MAR-2008.

[28] A. Donaldson, HWR-413 (1994).

[29] M. McGrath, Proceedings of the 2000 International Topical Meeting on LWR Fuel Performance (2000).